

Quantum Monte Carlo in Classical Phase Space with the Wigner-Kirkwood Commutation Function. II. Diagonal Approximation in Position Space.

Phil Attard

phil.attard1@gmail.com 13 Jan. 2026, March 4, 2026

A third order expansion for Wigner-Kirkwood commutation function, a complex function in classical phase space that accounts for the Heisenberg uncertainty relation, is approximated and integrated over momentum to give a real function in position configuration space. Metropolis Monte Carlo computer simulation results are given for liquid Lennard-Jones ^4He below 10 K.

I. INTRODUCTION

This paper follows on from Attard (2025h), which itself is based on earlier work (Attard 2016b, 2018b, 2021). The immediately preceding work presented computer simulation results in classical phase space for saturated liquid ^4He near the λ -transition, with certain quantum effects (ie. the Heisenberg uncertainty relation) included via a third order expansion of the Wigner-Kirkwood commutation function, which is both complex and a function of the momentum configuration. The purpose of the present paper is to explore an approximation that reduces the latter to a real function of position configuration space. There are certain practical and conceptual advantages to this, and there is apparently little loss of accuracy.

II. FORMALISM AND ALGORITHM

A. Phase Space Weight

For a subsystem of N identical bosons, a point in classical phase space is $\Gamma = \{\mathbf{q}, \mathbf{p}\}$. Here the position configuration is $\mathbf{q} = \{\mathbf{q}_1, \mathbf{q}_2, \dots, \mathbf{q}_N\}$ and the momentum configuration is $\mathbf{p} = \{\mathbf{p}_1, \mathbf{p}_2, \dots, \mathbf{p}_N\}$, where the position of boson j is $\mathbf{q}_j = \{q_{jx}, q_{jy}, q_{jz}\}$, and its momentum is $\mathbf{p}_j = \{p_{jx}, p_{jy}, p_{jz}\}$. Here we take the momentum to belong to the continuum; see Attard (2025a, 2025b) for the treatment of quantized momentum.

For a canonical equilibrium system of temperature T and volume V , the phase space probability density is (Attard 2018b, 2021)

$$\wp(\Gamma) = \frac{e^{-\beta\mathcal{H}(\Gamma)} e^{W(\Gamma)} \eta(\Gamma)}{N! h^{3N} Z}, \quad (2.1)$$

where h is Planck's constant, and $\beta = 1/k_B T$, k_B being Boltzmann's constant. The partition function, $Z(N, V, T)$, normalizes the probability and its logarithm gives the total entropy. Also the classical Hamiltonian is $\mathcal{H}(\Gamma) = \mathcal{K}(\mathbf{p}) + U(\mathbf{q})$, where $\mathcal{K}(\mathbf{p}) = p^2/2m = \sum_{j=1}^N p_j^2/2m$ is the kinetic energy, m being the mass of a boson. Below we shall take the potential energy to consist of central pair potentials $U(\mathbf{q}) = \sum_{j<k}^N u(q_{jk})$ and write $u_{jk} \equiv u(q_{jk})$.

The main focus of this work is on the Wigner-Kirkwood commutation function $W(\Gamma)$ (Attard 2018b, 2021, Kirkwood 1933, Wigner 1932), which is defined by

$$e^{-\beta\mathcal{H}(\Gamma)} e^{W(\Gamma)} = e^{\mathbf{p}\cdot\mathbf{q}/i\hbar} e^{-\beta\hat{\mathcal{H}}(\mathbf{q})} e^{-\mathbf{p}\cdot\mathbf{q}/i\hbar}. \quad (2.2)$$

This corresponds to $\omega_p = e^{W_p}$ (Attard 2018b Eq. (2.6)) (present notation). For the quantum weight one can use either $\omega_p \eta_q$ or else $\omega_q \eta_p$, with $\omega_q^* = \omega_p$ and $\eta_q^* = \eta_p$.

On the right hand side of the definition of the commutation function the Hamiltonian operator appears, $\hat{\mathcal{H}}(\mathbf{q}) = \hat{\mathcal{K}}(\mathbf{q}) + U(\mathbf{q})$. The Fourier factors are unnormalized, unsymmetrized momentum eigenfunctions. The non-zero commutator $[\hat{\mathcal{K}}, U] \neq 0$ is what makes $W \neq 0$, and so it reflects the Heisenberg uncertainty relation.

In the computational results for ^4He presented below the symmetrization function is neglected. This is appropriate on the high temperature side of the λ -transition. Our main aim is to delineate the rôle of the commutation function, and we shall take up the combined effects of the two in future work.

B. Fluctuation Expansion for the Commutation Function

Kirkwood (1933) took the inverse temperature derivative of the defining equation for the commutation function, Eq. (2.2), to obtain an infinite series in powers of β , explicitly giving the first non-zero term, which is quadratic in β . Higher order coefficients using this method have been obtained (Attard 2021 §§8.2–8.4).

A slightly different approach based on a fluctuation expansion has n th order coefficient (Attard 2021 §8.5)

$$\Delta_{\mathcal{H}}^{(n)}(\mathbf{q}, \mathbf{p}) \equiv \frac{\langle \mathbf{q} | [\hat{\mathcal{H}} - \mathcal{H}(\mathbf{q}, \mathbf{p})]^n | \mathbf{p} \rangle}{\langle \mathbf{q} | \mathbf{p} \rangle}. \quad (2.3)$$

One has $\Delta_{\mathcal{H}}^{(0)}(\mathbf{q}, \mathbf{p}) = 1$ and $\Delta_{\mathcal{H}}^{(1)}(\mathbf{q}, \mathbf{p}) = 0$. These give a series for the exponent of the form

$$W(\Gamma) = \frac{\beta^2}{2!} \tilde{\Delta}_{\mathcal{H}}^{(2)}(\Gamma) - \frac{\beta^3}{3!} \tilde{\Delta}_{\mathcal{H}}^{(3)}(\Gamma) + \frac{\beta^4}{4!} \tilde{\Delta}_{\mathcal{H}}^{(4)}(\Gamma) - \dots \quad (2.4)$$

The second order fluctuation, $\tilde{\Delta}_{\mathcal{H}}^{(2)} = \Delta_{\mathcal{H}}^{(2)}$, is

$$\Delta_{\mathcal{H}}^{(2)}(\mathbf{q}, \mathbf{p}) = \frac{-\hbar^2}{2m} \nabla^2 U(\mathbf{q}) - \frac{i\hbar}{m} \mathbf{p} \cdot \nabla U(\mathbf{q}). \quad (2.5)$$

The third order fluctuation, $\tilde{\Delta}_{\mathcal{H}}^{(3)} = \Delta_{\mathcal{H}}^{(3)}$, is

$$\begin{aligned} \Delta_{\mathcal{H}}^{(3)}(\mathbf{q}, \mathbf{p}) &= \frac{-\hbar^2}{m} \nabla U \cdot \nabla U + \frac{\hbar^4}{4m^2} \nabla^2 \nabla^2 U \\ &+ \frac{i\hbar^3}{m^2} \mathbf{p} \cdot \nabla \nabla^2 U - \frac{\hbar^2}{m^2} \mathbf{p} \mathbf{p} : \nabla \nabla U. \end{aligned} \quad (2.6)$$

Expressions for the gradients of a central pair potential have been catalogued (Attard 2021 §§9.5.2 and 9.5.3).

C. Momentum Integral in Diagonal Approximation

1. Pair Commutation Function

The real part of the second-order commutation function, which is independent of momentum, is

$$\begin{aligned} \tilde{W}_r^{(2)}(\mathbf{q}) &= \frac{\beta^2 - \hbar^2}{2} \frac{1}{2m} \nabla^2 U(\mathbf{q}) \\ &= \frac{-\beta^2 \hbar^2}{4m} \sum_{j < k} [\nabla_j^2 u_{jk} + \nabla_k^2 u_{jk}] \\ &= \frac{-\beta^2 \hbar^2}{4m} \sum_{j, k}^{(k \neq j)} \left[u''_{jk} + \frac{2u'_{jk}}{q_{jk}} \right]. \end{aligned} \quad (2.7)$$

Here and below $u'_{jk} = \partial u(q_{jk}) / \partial q_{jk}$, $u''_{jk} = \partial^2 u(q_{jk}) / \partial q_{jk}^2$, and similarly for higher order derivatives.

The imaginary momentum part of the second order fluctuation contributes

$$e^{iW_i^{(2)}} = e^{i \sum_{j=1}^N W_{i,j}^{(2)}/2}, \quad (2.8)$$

where the part involving boson j is

$$\begin{aligned} W_{i,j}^{(2)} &= \frac{-\beta^2 \hbar}{2m} [\mathbf{p} \cdot \nabla U(\mathbf{q})]_j \\ &= \frac{-\beta^2 \hbar}{2m} \sum_{k=1}^N \sum_{(k \neq j)} [\mathbf{p}_j \cdot \nabla_j u_{jk} + \mathbf{p}_k \cdot \nabla_k u_{jk}] \\ &= \frac{-\beta^2 \hbar}{2m} \sum_{k=1}^N \sum_{(k \neq j)} \left[\frac{\mathbf{p}_j \cdot \mathbf{q}_{jk}}{q_{jk}} u'_{jk} + \frac{\mathbf{p}_k \cdot \mathbf{q}_{kj}}{q_{kj}} u'_{kj} \right] \\ &= \frac{-\beta^2 \hbar}{2m} \sum_{k=1}^N \sum_{(k \neq j)} \frac{\mathbf{p}_{jk} \cdot \mathbf{q}_{jk}}{q_{jk}} u'_{jk}. \end{aligned} \quad (2.9)$$

This has to be divided by two in the total because it counts each pair interaction twice when summed over j . Writing the total dependence on j is useful for the Metropolis Monte Carlo step.

We can write the total of this contribution as

$$\begin{aligned} W_i^{(2)} &= \prod_{j < k} e^{(-i\beta^2 \hbar u'_{jk} / 2mq_{jk}) \mathbf{p}_{jk} \cdot \mathbf{q}_{jk}} \\ &= \prod_{j < k} e^{(-i\beta^2 \hbar u'_{jk} / 2mq_{jk}) [\mathbf{p}_j \cdot \mathbf{q}_{jk} + \mathbf{p}_k \cdot \mathbf{q}_{kj}]} \\ &= \prod_{j, k}^{(k \neq j)} e^{(-i\beta^2 \hbar u'_{jk} / 2mq_{jk}) \mathbf{p}_j \cdot \mathbf{q}_{jk}} \\ &= \prod_j e^{-i\mathbf{a}_j \cdot \mathbf{p}_j / \hbar}, \end{aligned} \quad (2.10)$$

where the corresponding ‘position’ is

$$\mathbf{a}_j(\mathbf{q}) \equiv \frac{\beta^2 \hbar^2}{2m} \sum_{k=1}^N \sum_{(k \neq j)} \frac{u'_{jk}}{q_{jk}} \mathbf{q}_{jk}. \quad (2.11)$$

The magnitude of each pair contribution to this is large in the core region, and it goes to zero at large separations. With it the momentum integral is

$$\begin{aligned} I_{W2} &= \frac{1}{h^{3N}} \int d\mathbf{p} e^{-\beta p^2 / 2m} \prod_{j=1}^N e^{-\mathbf{a}_j \cdot \mathbf{p}_j / i\hbar} \\ &= \frac{1}{h^{3N}} \prod_{j=1}^N \int d\mathbf{p}_j e^{-\beta p_j^2 / 2m} e^{-\mathbf{a}_j \cdot \mathbf{p}_j / i\hbar} \\ &= \Lambda^{-3N} \prod_{j=1}^N e^{-\pi \mathbf{a}_j(\mathbf{q})^2 / \Lambda^2}. \end{aligned} \quad (2.12)$$

The thermal wavelength is $\Lambda = \sqrt{2\pi \hbar^2 \beta / m}$. Since a_j is large at small separations, this keeps particle j more separated from its neighbors than in the classical case, which is to say in the absence of the Wigner-Kirkwood commutation function.

2. Triplet Commutation Function

For the third order fluctuation, there are two terms that are independent of momentum. The first is

$$\begin{aligned} \tilde{W}_{r,a}^{(3)} &= \frac{-\beta^3 - \hbar^2}{3!} \frac{1}{m} \nabla U \cdot \nabla U \\ &= \frac{\beta^3 \hbar^2}{3!m} \sum_{j=1}^N \sum_{k, k'} \nabla_j u_{jk} \cdot \nabla_j u_{jk'} \\ &= \frac{\beta^3 \hbar^2}{3!m} \sum_{j=1}^N \mathbf{g}_j \cdot \mathbf{g}_j, \end{aligned} \quad (2.13)$$

where

$$\mathbf{g}_j \equiv \sum_{k=1}^N \sum_{(k \neq j)} \nabla_j u_{jk} = \sum_{k=1}^N \sum_{(k \neq j)} \frac{u'_{jk}}{q_{jk}} \mathbf{q}_{jk}. \quad (2.14)$$

Note that \mathbf{g}_j depends upon \mathbf{q}_j and also \mathbf{q}_k for k within the potential cut-off neighborhood of j . This must be taken into account in the Metropolis Monte Carlo step.

The second real momentum-independent part is

$$\begin{aligned}\tilde{W}_{r,b}^{(3)} &= \frac{-\beta^3}{3!} \frac{\hbar^4}{4m^2} \nabla^2 \nabla^2 U \\ &= \frac{-\beta^3 \hbar^4}{12m^2} \sum_{j,k}^{(k \neq j)} \left\{ u_{jk}^{iv} + \frac{4u_{jk}'''}{q_{jk}} \right\}. \quad (2.15)\end{aligned}$$

The momentum-dependent terms in the third order fluctuation are an imaginary term linear in momentum, $(i\hbar^3/m^2)\mathbf{p} \cdot \nabla \nabla^2 U$ and a real term that is quadratic in momentum $(-\hbar^2/m^2)\mathbf{p}\mathbf{p} : \nabla \nabla U$. These are multiplied by $-\beta^3/3!$.

In time-honored tradition, for the quadratic momentum term we neglect the ‘difficult’ off-diagonal terms, $\mathbf{p}_j \mathbf{p}_k$. The justification is that these can be positive or negative and therefore they largely cancel. In fact the first neglected term that is non-zero on average is $\mathcal{O}(p^4)$, which is small at low temperatures, more so in the quantum than the classical case. In view of this we keep only the leading terms even in momentum, which gives the diagonal approximation, namely

$$\begin{aligned}W_{r,c}^{(3)} &= \frac{-\beta^3}{3!} \frac{-\hbar^2}{m^2} \mathbf{p}\mathbf{p} : \nabla \nabla U \\ &\approx \frac{\beta^3 \hbar^2}{6m^2} \sum_{j,\alpha} p_{j\alpha}^2 \partial_{j\alpha}^2 U \\ &= \frac{\beta^3 \hbar^2}{6m^2} \sum_{j,\alpha} \sum_k^{(j \neq k)} p_{j\alpha}^2 \partial_{j\alpha}^2 u_{jk} \\ &= \frac{\beta^3 \hbar^2}{6m^2} \sum_{j,\alpha} \sum_k^{(j \neq k)} p_{j\alpha}^2 \\ &\quad \times \left[\frac{u_{jk}'' q_{jk,\alpha}^2}{q_{jk}^2} - \frac{u_{jk}' q_{jk,\alpha}^2}{q_{jk}^3} + \frac{u_{jk}'}{q_{jk}} \right] \\ &\equiv \sum_{j=1}^N \sum_{\alpha=x,y,z} B_{j\alpha}(\mathbf{q}) p_{j\alpha}^2, \quad (2.16)\end{aligned}$$

where

$$\begin{aligned}B_{j\alpha}(\mathbf{q}) &\equiv \frac{\beta^3 \hbar^2}{6m^2} \sum_{k=1}^N \sum_{(k \neq j)} \left\{ \frac{u_{jk}'' q_{jk,\alpha}^2}{q_{jk}^2} - \frac{u_{jk}' q_{jk,\alpha}^2}{q_{jk}^3} + \frac{u_{jk}'}{q_{jk}} \right\} \\ &\equiv \sum_{k \in \mathcal{N}_j} B_{k\alpha}^{(j)}. \quad (2.17)\end{aligned}$$

Here \mathcal{N}_j is a list of the bosons within the potential cut-off neighborhood of j . The quantity $B_{k\alpha}^{(j)}$ is the contribution of boson k to $B_{j\alpha}$, and it can be used to calculate the change in the latter with a change in \mathbf{q}_k , and *vice versa* for $B_{j\alpha}^{(k)}$. The quantity $B_{j\alpha}$ will combine with the classical kinetic energy to give an effective inverse temperature for each boson momentum component, $\beta_{j\alpha} = \beta - 2mB_{j\alpha}$.

The imaginary part is

$$\begin{aligned}W_i^{(3)} &= \frac{-\beta^3}{3!} \frac{\hbar^3}{m^2} \mathbf{p} \cdot \nabla \nabla^2 U \quad (2.18) \\ &= \frac{-\beta^3 \hbar^3}{3!m^2} \sum_{j,k} \mathbf{p}_j \cdot \nabla_j \nabla_j^2 u_{jk} \\ &= \frac{-\beta^3 \hbar^3}{3!m^2} \sum_{j,k} \mathbf{p}_j \cdot \nabla_j [\nabla_j^2 + \nabla_k^2] u_{jk} \\ &= \frac{-2\beta^3 \hbar^3}{3!m^2} \sum_{j,k} \mathbf{p}_j \cdot \nabla_j \nabla_j^2 u_{jk} \\ &= \frac{-2\beta^3 \hbar^3}{3!m^2} \sum_{j,k}^{(k \neq j)} \left[\frac{u_{jk}'''}{q_{jk}} + \frac{2u_{jk}''}{q_{jk}^2} - \frac{2u_{jk}'}{q_{jk}^3} \right] \mathbf{p}_j \cdot \mathbf{q}_{jk}.\end{aligned}$$

This contribution to the weight is

$$\begin{aligned}e^{iW_i^{(3)}(\mathbf{p},\mathbf{q})} &= \prod_{j,k} e^{(-i\beta^3 \hbar^3/3m^2) \left[\frac{u_{jk}'''}{q_{jk}} + \frac{2u_{jk}''}{q_{jk}^2} - \frac{2u_{jk}'}{q_{jk}^3} \right] \mathbf{p}_j \cdot \mathbf{q}_{jk}} \\ &\equiv \prod_j e^{-i\mathbf{b}_j \cdot \mathbf{p}_j / \hbar}, \quad (2.19)\end{aligned}$$

where the third order ‘position’ is

$$\mathbf{b}_j(\mathbf{q}) \equiv \frac{\hbar^4 \beta^3}{3m^2} \sum_{k=1}^N \sum_{(k \neq j)} \left[\frac{u_{jk}'''}{q_{jk}} + \frac{2u_{jk}''}{q_{jk}^2} - \frac{2u_{jk}'}{q_{jk}^3} \right] \mathbf{q}_{jk}. \quad (2.20)$$

Everything goes through as for the pair term with $\beta \Rightarrow \beta_{j\alpha}$, $\Lambda \Rightarrow \Lambda_{j\alpha}$ and $\mathbf{a}_j \Rightarrow \mathbf{a}_j + \mathbf{b}_j$. Thus the momentum integral for the average of the second and third order terms is

$$\begin{aligned}I_{W3} &= \frac{1}{h^{3N}} \int d\mathbf{p} e^{-\beta p^2/2m} \\ &\quad \times \prod_{j,\alpha} \left[e^{-i\mathbf{a}_{j\alpha} \mathbf{p}_{j\alpha} / \hbar} e^{B_{j\alpha} p_{j\alpha}^2} e^{-i\mathbf{b}_{j\alpha} \mathbf{p}_{j\alpha} / \hbar} \right] \\ &= \prod_{j,\alpha} \left[\Lambda_{j\alpha}^{-1} e^{-\pi c_{j\alpha}^2 / \Lambda_{j\alpha}^2} \right]. \quad (2.21)\end{aligned}$$

Here and below $c_{j\alpha} \equiv a_{j\alpha} + b_{j\alpha}$, $\beta_{j\alpha} \equiv \beta - 2mB_{j\alpha}$, and $\Lambda_{j\alpha} \equiv \sqrt{2\pi\hbar^2\beta_{j\alpha}/m}$.

In summary, the position configuration space weight in the third order diagonal approximation is

$$\wp_{\text{diag}}^{(3)}(\mathbf{q}) = \frac{e^{-\beta U(\mathbf{q})} e^{\tilde{W}_r(\mathbf{q})}}{N!Z} \prod_{j,\alpha} \frac{e^{-\pi c_{j\alpha}(\mathbf{q})^2 / \Lambda_{j\alpha}(\mathbf{q})^2}}{\Lambda_{j\alpha}(\mathbf{q})}. \quad (2.22)$$

Here $\tilde{W}_r = \tilde{W}_r^{(2)} + \tilde{W}_r^{(3)} + \tilde{W}_{r,b}^{(3)}$. The partition function is

$$\begin{aligned}Z(N, V, T) &= \frac{1}{N!} \int d\mathbf{q} e^{-\beta U(\mathbf{q})} e^{\tilde{W}_r(\mathbf{q})} \prod_{j,\alpha} \frac{e^{-\pi c_{j\alpha}(\mathbf{q})^2 / \Lambda_{j\alpha}(\mathbf{q})^2}}{\Lambda_{j\alpha}(\mathbf{q})}. \quad (2.23)\end{aligned}$$

D. Metropolis Monte Carlo Step

The classical Metropolis Monte Carlo algorithm for pair potentials can be very efficient if neighbor tables are used, in which case it scales linearly with the number of particles N . Some, but not all, of the terms in the present position-dependent commutation function are the sum of pair terms, and so they fit naturally into existing schemes. Careful attention has to be paid to the term that is the product of gradients of the potential, and to the momentum-derived terms in order to compute the Metropolis Monte Carlo step efficiently.

We can write $\mathbf{c}_j \equiv \mathbf{a}_j + \mathbf{b}_j = \sum_k^{(k \neq j)} f_{jk} \mathbf{q}_{jk}$ where

$$f_{jk} = \frac{\beta^2 \hbar^2}{2m} \frac{u'_{jk}}{q_{jk}} + \frac{\beta^3 \hbar^4}{3m^2} \left[\frac{1}{q_{jk}} u'''_{jk} + \frac{2}{q_{jk}^2} u''_{jk} - \frac{2}{q_{jk}^3} u'_{jk} \right]. \quad (2.24)$$

The momentum-integrated Gaussian exponent is

$$W_p(\mathbf{q}) = -\pi \sum_{j,\alpha} \frac{c_{j\alpha}^2}{\Lambda_{j\alpha}^2}. \quad (2.25)$$

For a trial move $\mathbf{q}_j \Rightarrow \mathbf{q}'_j$, the change in this is

$$\Delta_{j\alpha} W_p = \frac{-\pi c_{j\alpha}^{\prime 2}}{\Lambda_{j\alpha}^2} + \frac{\pi c_{j\alpha}^2}{\Lambda_{j\alpha}^2} - \pi \sum_{k \in \mathcal{N}_j} \left\{ \frac{c_{k\alpha}^{\prime 2}}{\Lambda_{k\alpha}^2} - \frac{c_{k\alpha}^2}{\Lambda_{k\alpha}^2} \right\}. \quad (2.26)$$

Here \mathcal{N}_j is a list of the bosons within the potential cut-off neighborhood of j . We have

$$c'_{k\alpha} = c_{k\alpha} + f_{jk} q'_{jk,\alpha} - f_{jk} q_{jk,\alpha}, \quad (2.27)$$

and

$$\Lambda_{k\alpha}^{\prime 2} = \frac{2\pi \hbar^2}{m} \left\{ \beta - 2m \left[B_{k\alpha} + B_{j\alpha}^{(k)'} - B_{j\alpha}^{(k)} \right] \right\}. \quad (2.28)$$

These require $\mathcal{O}(\mathcal{N}_j)$ terms to be computed for each change in position, which is the same as for the pair potential.

The change in the pre-exponential factor of the weight, $\prod_{j,\alpha} \Lambda_{j,\alpha}(\mathbf{q})^{-1}$ also follows from this last result.

Similar techniques can be used for the third order real term that is quadratic in the potential. The change in this for $\mathbf{q}_j \Rightarrow \mathbf{q}'_j$ is

$$\Delta_j \tilde{W}_{r,a}^{(3)} = \frac{\beta \hbar^2}{3!m} \left\{ \sum_{\alpha} [g_{j\alpha}^{\prime 2} - g_{j\alpha}^2] + \sum_{k \in \mathcal{N}_j} \sum_{\alpha} \left[\left(g_{k\alpha} + g_{j\alpha}^{(k)'} - g_{j\alpha}^{(k)} \right)^2 - g_{k\alpha}^2 \right] \right\}. \quad (2.29)$$

Here the j -dependent contribution to \mathbf{g}_k is

$$\mathbf{g}_j^{(k)} = \frac{u'_{jk}}{q_{jk}} \mathbf{q}_{kj}. \quad (2.30)$$

Again it takes on the order of \mathcal{N}_j terms to evaluate the change, which is the same as for the pair potential itself.

E. Average Energy and Heat Capacity

As above we write $\mathbf{c}_j \equiv \mathbf{a}_j + \mathbf{b}_j = \sum_k^{(k \neq j)} f_{jk} \mathbf{q}_{jk}$, where the above expression shows that $f_{jk} \equiv \beta^2 f_{jk}^{(2)} + \beta^3 f_{jk}^{(3)}$. Using an over-dot to denote the inverse temperature derivative, we have $\dot{f}_{jk} = 2\beta f_{jk}^{(2)} + 3\beta^2 f_{jk}^{(3)}$ and $\ddot{f}_{jk} = 2f_{jk}^{(2)} + 6\beta f_{jk}^{(3)}$. Hence $\dot{c}_{j\alpha}$ and $\ddot{c}_{j\alpha}$ follow. Since $B_{j\alpha} \propto \beta^3$, $\dot{B}_{j\alpha} = 3B_{j\alpha}/\beta$ and $\ddot{B}_{j\alpha} = 6B_{j\alpha}/\beta^2$. And since $\beta_{j\alpha}(\mathbf{q}) \equiv \beta - 2mB_{j\alpha}(\mathbf{q})$, then $\dot{\beta}_{j\alpha} = 1 - 2m\dot{B}_{j\alpha}$, and $\ddot{\beta}_{j\alpha} = -2m\ddot{B}_{j\alpha}$. The derivatives of $\Lambda_{j\alpha}(\mathbf{q}) = \sqrt{2\pi\beta_{j\alpha}\hbar^2/m}$ also follow.

The negative of the temperature-dependent exponent of the position configuration probability is

$$H^{\S}(\mathbf{q}) \equiv \beta U(\mathbf{q}) - \tilde{W}_r(\mathbf{q}) + \pi \sum_{j,\alpha} \frac{c_{j,\alpha}(\mathbf{q})^2}{\Lambda_{j,\alpha}(\mathbf{q})^2} + \sum_{j,\alpha} \ln \Lambda_{j,\alpha}(\mathbf{q}). \quad (2.31)$$

The thermal wavelength that appears as the argument of the logarithm has the same unit of length as the position configuration, but this is not important for the derivatives. The inverse temperature derivative of this is a sort of statistical energy or enthalpy,

$$\begin{aligned} H(\mathbf{q}) &\equiv \frac{\partial H^{\S}(\mathbf{q})}{\partial \beta} \\ &= U - \dot{\tilde{W}}_r + \sum_{j,\alpha} \left\{ \frac{2\pi \dot{c}_{j,\alpha} c_{j,\alpha}}{\Lambda_{j,\alpha}^2} - \frac{\pi c_{j,\alpha}^2}{\beta_{j\alpha} \Lambda_{j,\alpha}^2} \dot{\beta}_{j\alpha} + \frac{\dot{\beta}_{j\alpha}}{2\beta_{j,\alpha}} \right\}. \end{aligned} \quad (2.32)$$

The monomer thermodynamic energy is

$$\overline{E}^{(1)} = \frac{-\partial \ln Z}{\partial \beta} = \langle H \rangle. \quad (2.33)$$

The heat capacity is $C_V = \partial \overline{E}^{(1)} / \partial T = -k_B \beta^2 \partial \overline{E}^{(1)} / \partial \beta$. We have

$$\frac{\partial \overline{E}^{(1)}}{\partial \beta} = \langle H \rangle^2 - \langle H^2 - \dot{H} \rangle = \langle \dot{H} - [H - \langle H \rangle]^2 \rangle, \quad (2.34)$$

with

$$\begin{aligned} \dot{H} &= -\ddot{\tilde{W}}_r + \sum_{j,\alpha} \left\{ \frac{2\pi \ddot{c}_{j,\alpha} c_{j,\alpha} + 2\pi \dot{c}_{j,\alpha}^2}{\Lambda_{j,\alpha}^2} - \frac{2\pi \dot{c}_{j,\alpha} c_{j,\alpha}}{\beta_{j,\alpha} \Lambda_{j,\alpha}^2} \dot{\beta}_{j\alpha} - \frac{2\pi \dot{c}_{j,\alpha} c_{j,\alpha}}{\beta_{j,\alpha} \Lambda_{j,\alpha}^2} \dot{\beta}_{j\alpha} + \frac{2\pi c_{j,\alpha}^2}{\beta_{j,\alpha}^2 \Lambda_{j,\alpha}^2} \dot{\beta}_{j\alpha}^2 - \frac{\pi c_{j,\alpha}^2}{\beta_{j,\alpha} \Lambda_{j,\alpha}^2} \ddot{\beta}_{j\alpha} + \frac{\ddot{\beta}_{j\alpha}}{2\beta_{j,\alpha}} - \frac{\dot{\beta}_{j,\alpha}^2}{2\beta_{j,\alpha}^2} \right\}. \end{aligned} \quad (2.35)$$

F. Kinetic Energy

The kinetic energy as a function of the position configuration in the third order, diagonal approximation is

$$\mathcal{K}(\mathbf{q}) = \frac{1}{2} \sum_{k=1}^N \sum_{\gamma=x,y,z} \beta_{k\gamma}(\mathbf{q})^{-1}. \quad (2.36)$$

The average of this is expected to be less than the classical average kinetic energy, $\overline{\mathcal{K}}^{\text{cl}} = 3N/2\beta$.

G. Symmetrization Function

It is a relatively minor matter to include the symmetrization function in the present third order diagonal approximation. It simply requires the replacement $\Lambda \Rightarrow \Lambda_{j\alpha}$. From earlier work (Attard 2018b, 2021), the symmetrization l -loop grand potential is given by

$$-\beta\Omega^{(l)} = \left\langle \eta^{(l)}(\mathbf{\Gamma}) \right\rangle, \quad (2.37)$$

where the l -loop symmetrization function is

$$\eta^{(l)}(\mathbf{\Gamma}) = \sum_{j_1, \dots, j_l}^N \prod_{k=1}^l e^{-\mathbf{p}_{j_k} \cdot \mathbf{q}_{j_k, j_{k+1}} / i\hbar}, \quad j_{l+1} \equiv j_1. \quad (2.38)$$

The sum is over the unique directed cyclic permutations of all subsets of l -bosons. Using the third order diagonal approximation the momentum quadrature reduces this to

$$\eta^{(l)}(\mathbf{q}) = \sum_{j_1, \dots, j_l}^N \prod_{k=1}^l \prod_{\alpha=x,y,z} e^{-\pi(q_{j_k j_{k+1}, \alpha} - c_{j_k \alpha})^2 / \Lambda_{j_k \alpha}^2}. \quad (2.39)$$

III. COMPUTATIONAL RESULTS

A. Model and Simulation Details

Metropolis Monte Carlo simulations were performed in configuration position space using the third order diagonal approximation for the Wigner-Kirkwood commutation function. The Lennard-Jones pair potential was used, $u(r) = 4\varepsilon[(\sigma/r)^{12} - (\sigma/r)^6]$, with helium parameters, $\varepsilon_{\text{He}} = 10.22k_{\text{B}} \text{ J}$ and $\sigma_{\text{He}} = 0.2556 \text{ nm}$ (van Sciver 2012). The potential was cut off at $R_{\text{cut}} = 3.5\sigma$. Periodic boundary conditions were used together with the nearest neighbor convention. A small cell spatial neighborhood was used. The position steps for a trial configuration were chosen to give acceptance rates of 30–60%. Usually $N = 1,000$ atoms were used, and these formed a homogeneous fluid.

TABLE I: Quantum Monte Carlo in classical phase space with numerical momentum quadrature (Attard 2025h). Results for Lennard-Jones ^4He using $N = 1,000$, full momentum quadrature, $n_w^{\text{max}} = 3$, and $|W_i| < \pi/2$, unless otherwise indicated. The statistical error in the final digit shown in parentheses is at the 95% confidence level.

$k_{\text{B}}T/\varepsilon$	$\rho\sigma^3$	$\beta\overline{\mathcal{K}}/N$	$\beta\overline{E}/N$	C_V/Nk_{B}
0.50	0.26	0.8538(2)	-10.988(2)	28.8(3)
0.50 ^a	0.26	0.8544(2)	-10.983(4)	29.0(5)
0.50 ^b	0.26	0.850(9)	-11.00(6)	—
0.50 ^c	0.26	0.6508(2)	-11.947(4)	27.2(3)
0.50 ^d	0.26	0.455(1)	28.7(5)	-69(11)
0.49	0.26	0.8429(4)	-11.816(4)	30.5(3)
0.49 ^d	0.26	0.441(1)	30.8(6)	-81(2)
0.45	0.26	0.7935(3)	-15.917(6)	38.9(4)
0.40	0.26	0.7225(7)	-23.67(1)	55.1(9)
0.35	0.26	0.633(2)	-36.9(1)	120(25)

^a $N = 2,000$. ^bUmbrella sampling, $e^{-W_i^2/2}$. ^cDiagonal approximation. ^d $n_w^{\text{max}} = 4$.

B. Results

1. Numerical Momentum Quadrature

Table I provides benchmark results obtained with the previous computer simulation algorithm in which the momentum integrals were evaluated by Metropolis Monte Carlo quadrature. These results supersede those in versions 1 and 2 of Attard (2025h).

The result are for a homogeneous fluid of density $\rho\sigma^3 = 0.26$. This is the liquid saturation density of ^4He at $k_{\text{B}}T/\varepsilon = 0.5$, as estimated from the measured data (Donnelly and Barenghi, 1998). The second entry shows that the algorithm is relatively insensitive to the size of the system.

The umbrella sampling method removes the constraint $|W_i| < \pi/2$ and replaces the weight $\cos W_i$ with $e^{-W_i^2/2}$ in the Metropolis Monte Carlo step, and corrects for this in the averaging step with the factor $e^{W_i^2/2} \cos W_i$. This comes at the cost of greater statistical error, most markedly for the heat capacity where it was about 4 orders of magnitude larger than for direct sampling for the same length simulation. Nevertheless the agreement of the umbrella sampling results with the direct results for the kinetic energy and for the thermodynamic energy suggests that the constraint $|W_i| < \pi/2$ has no deleterious consequences.

The results at $k_{\text{B}}T/\varepsilon = 0.49$ give the numerical derivative $\Delta\overline{E}/\Delta T = 29.6(2)$, which is in good agreement with the heat capacity simulated directly, which was obtained using the formula in version 1 of Attard (2025h). This is a sensitive test for computer bugs. It also confirms that the results are insensitive to the constraint $|W_i| < \pi/2$.

The fourth entry in Table I shows that the diagonal approximation is relatively accurate. For these results the

momenta still appeared explicitly and the momentum integrals were still evaluated using the Metropolis Monte Carlo method. The only difference was that Eq. (2.16) was used instead of the full expression. The approximation underestimates the kinetic energy by about 25%, overestimates the magnitude of the energy by about 10%, and underestimates the heat capacity by about 5%. It can be concluded that this approximation is relatively reliable.

The fifth and seventh entries in Table I use the fourth order expansion, $n_w^{\max} = 4$. In these simulations there were indications of slow equilibration and of solidification, and the diffusion over their course was extremely limited, with the average change in separation of a pair of atoms being 0.1σ . The thermodynamic phase of Lennard-Jones ^4He is sensitive to the order of the expansion for the commutation function, and so the quantitative results at this density and temperature should be treated with caution. It is problematic to compare these fourth order results that yield a solid-like phase with the third order results that give a fluid phase. For what it is worth, it can be seen that at $k_B T/\varepsilon = 0.50$, compared to the third order expansion, the kinetic energy is substantially smaller and the statistical enthalpy is substantially more positive. The heat capacity given by the fourth order expansion is large in magnitude and negative in sign, which indicates that the state is thermodynamically unstable. The numerical difference in thermodynamic energy for these two states was $\Delta\bar{E}/\Delta T = -75(38)$, which is consistent with the heat capacities obtained by direct simulation. Runs at $k_B T/\varepsilon = 0.50$ and $\rho\sigma^3 = 0.20$ appear to have equilibrated as solids with $\beta\bar{K}/N = 0.617(2)$, $\beta\bar{E}/N = -4.6(1)$, and $C_V/Nk_B = 36.3(14)$.

One can conclude that at these temperatures and densities Lennard-Jones ^4He is close to coexisting solid, liquid, and vapor phases. One therefore expects that the structure and the dynamics of the system would be sensitive to the details of the model intermolecular potential and to the order of the expansion for the Wigner-Kirkwood commutation function. The proximity of model ^4He to the phase boundaries makes it challenging to obtain reliable quantitative results that can be compared to real ^4He .

2. Analytic Diagonal Approximation

Table II shows the results of the present quantum Monte Carlo simulations in third order diagonal approximation in position configuration space. The fixed density $\rho\sigma^3 = 0.26$, which is the liquid saturation density at $k_B T/\varepsilon = 0.5$, underestimates the saturation density at lower temperatures, being about 25% less than the measured saturation value at the lowest temperature simulated, $\rho^{\text{sat}}\sigma^3 = 0.34$ at $k_B T/\varepsilon = 0.35$. An attempt was made to use the saturation density measured at each temperature, but it was found that the system solidified for $k_B T/\varepsilon \leq 0.45$. For all temperatures at $\rho\sigma^3 = 0.26$, the

TABLE II: Simulation results in position configuration space using the third order diagonal analytic approximation for the momentum.

$k_B T/\varepsilon$	$\rho\sigma^3$	Λ/σ	$\bar{\Lambda}_{j\alpha}/\sigma$	$\beta\bar{K}/N$	$\beta\bar{E}/N$	C_V/Nk_B
1.0	0.26	1.0679	1.244(1)	1.105(2)	1.0745(8)	4.98(5)
0.9	0.26	1.1257	1.350(2)	1.043(3)	0.5804(5)	6.11(9)
0.8	0.26	1.1940	1.486(1)	0.968(1)	-0.226(1)	8.0(1)
0.7	0.26	1.2764	1.667(2)	0.880(3)	-1.613(2)	11.10(4)
0.6	0.26	1.3787	1.921(2)	0.772(2)	-4.160(1)	16.8(1)
0.5	0.26	1.5103	2.300(2)	0.6467(9)	-9.291(2)	27.3(2)
0.49	0.26	1.5256	2.349(3)	0.629(2)	-10.054(2)	29.2(1)
0.45	0.26	1.5920	2.570(1)	0.575(1)	-13.850(3)	36.6(1)
0.4	0.26	1.6886	2.929(3)	0.498(4)	-20.987(3)	50.8(1)
0.35	0.26	1.8051	3.42(2)	0.422(8)	-32.76(3)	78.0(9)

system appeared to be a stable fluid, except for the lowest temperature, $k_B T/\varepsilon = 0.35$, where the simulated system was a metastable fluid that eventually transformed to a solid for longer simulations.

It can be seen in Table II that the effective thermal wavelength $\bar{\Lambda}_{j\alpha}/\sigma$ averaged over all particles and components is larger than the classical value, increasingly so as the temperature decreases. It is almost twice the size of the classical thermal wavelength at the lowest temperature studied. This is a manifestation of the fact that the effective temperature in the quantum system is less than the applied temperature. This is an unusual and unexpected consequence of the Heisenberg uncertainty relation as manifest in the Wigner-Kirkwood commutation function. Since the λ -transition occurs when $\rho\Lambda^3 = \mathcal{O}(1)$, that the effective thermal wavelength is larger than the classical value means that the transition will occur at higher temperatures than would have been predicted on the basis of classical considerations.

A closely related quantity is the kinetic energy per particle, which in Table II can be seen to be much less than the classical value, $\beta\mathcal{K}^{\text{cl}}/N = 3/2$. Again this can be interpreted as the effective temperature of the quantum system being much less than the reservoir temperature. Alternatively, one can say that the bosons occupy lower momentum states than would be predicted by classical considerations.

The kinetic energy per particle listed in Table II is actually $3\Lambda^2/2\bar{\Lambda}_{j\alpha}^2$. This is approximately the same as the exact result, Eq. (2.36). At the temperature $k_B T/\varepsilon = 0.5$, the result in the table is $\beta\mathcal{K}/N = 0.6467(9)$, whereas the result of Eq. (2.36) is $0.66122(5)$. This can be compared with the numerical third order diagonal approximation in Table I, namely $0.6508(2)$, and with the full numerical benchmark, $0.8538(2)$. There is a statistically significant difference of 1–2% between the analytic (Table I) and the numerical (Table II) third order diagonal approximations, the origin of which is unclear. Possibly it reflects a limitation of the constraint $|W_i| < \pi/2$ that is applied in the numerical quadrature, but not in the analysis.

Table II also shows the average thermodynamic energy and the specific heat capacity from the simulations. The heat capacity is positive, as it must be, and it increases with decreasing temperature. This is the opposite trend to that which is measured in the laboratory, where the heat capacity decreases with decreasing temperature prior to diverging at the λ -transition. (The present results are on a constant density curve, whereas the experimental results are on the saturation curve.) The lowest temperature in the table is about 1.4 K above the λ -transition at $T_\lambda = 2.18$ K. Since symmetrization effects are not here included, the present increase in heat capacity with decreasing temperature is unlikely to have anything to do with the measured divergence at the λ -transition. Instead it likely reflects the approach to the liquid-solid transition in the simulated system.

The minimum specific heat capacity on the saturation curve prior to the λ -transition is 9.04 J/mol K at 2.55 K (Donnelly and Barenghi 1998). In the present dimensionless units this is $C_s/Nk_B = 1.09$ at $k_B T/\varepsilon = 0.25$. This is much lower than the simulation results in Table II. It is not expected that the difference between the heat capacity at constant saturation and the heat capacity at constant volume could account for this discrepancy. It is more likely that the larger than expected heat capacity is due to the proximity to the liquid-solid transition in the present model.

The present results for the third order analytic diagonal approximation for $k_B T/\varepsilon = 0.50$ and $\rho\sigma^3 = 0.26$ are $\beta E/N = -9.292(2)$ and $-\beta^2 \dot{E}/N = 27.4(2)$. For $k_B T/\varepsilon = 0.49$ and $\rho\sigma^3 = 0.26$, $\beta E/N = -10.054(2)$ and $-\beta^2 \dot{E}/N = 29.2(1)$ (Table II). From these energies, the numerical derivative is $\Delta E/Nk_B \Delta T = 28.0(2)$. That this agrees with the directly simulated heat capacity is a very sensitive test of the mathematical expressions for the energy and the heat capacity, and of their computer implementation. It also tests the Metropolis Monte Carlo algorithm and its implementation. The author can attest to the sensitivity of the procedure as it took many rounds of debugging to get quantitative agreement between the two.

The agreement of the present results for the energy and the heat capacity with the earlier more exact simulations tends to confirm the utility of the diagonal approximation. This conclusion must be balanced against the disagreement in the kinetic energy pinpointed above.

Figure 1 compares the radial distribution function obtained with the present third order diagonal approximation with that obtained with the numerical full momentum quadrature. It can be seen that the two are in relatively close agreement. This suggests that for structural properties at least the diagonal approximation is quite good. This possibly explains the good agreement for the energy and the heat capacity discussed above. Also shown in the figure is the classical result at the higher density $\rho\sigma^3 = 0.9331$, which is the classical Lennard-Jones ^4He saturation density at $k_B T/\varepsilon = 0.5$. The most noticeable change is the increases in the size of the core

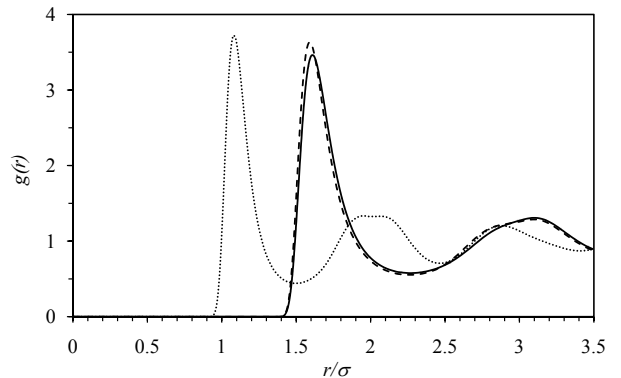


FIG. 1: Radial distribution function for Lennard-Jones ^4He at $k_B T/\varepsilon = 0.5$ and $\rho\sigma^3 = 0.26$. The solid curve is the present third order diagonal approximation, the dashed curve is the full third order with numerical momentum quadrature, and the dotted curve is the classical result at $\rho\sigma^3 = 0.9331$.

or exclusion region in the quantum system. This is evidently a direct result of the Wigner-Kirkwood commutation function, and it can be interpreted as a manifestation of the Heisenberg uncertainty relation.

A better measure of the location of the λ -transition than $\rho\Lambda^3 = \mathcal{O}(1)$ is arguably $\bar{\Lambda}_{j\alpha}/r_{\text{peak}} \gtrsim 1$, where r_{peak} gives the peak of the radial distribution function. (Or $\rho g_{\text{peak}} 2\pi r_{\text{peak}}^2 \Delta_{\text{peak}} e^{-\pi r_{\text{peak}}^2/\bar{\Lambda}_{j\alpha}^2} \gtrsim 1$.) For the classical Lennard-Jones fluid, $r_{\text{peak}}^{\text{cl}} \lesssim 2^{1/6}\sigma = 1.1\sigma$, and $\Lambda/r_{\text{peak}}^{\text{cl}} = 1.5/1.1 = 1.4$ at $k_B T/\varepsilon = 0.5$. In the quantum case in Fig. 1, $r_{\text{peak}} = 1.58\sigma$, $g_{\text{peak}} = 3.62$, and $\bar{\Lambda}_{j\alpha} = 2.3\sigma$, giving $\bar{\Lambda}_{j\alpha}/r_{\text{peak}} = 1.4$. This is about the same as the classical estimate. (For $n_w^{\text{max}} = 4$, $r_{\text{peak}} = 1.69\sigma$ and $g_{\text{peak}} = 6.90$.) Of course this is a rather crude estimate of the transition, and the two quantities have different rates of change with temperature. Nevertheless it suggests that the commutation function contributes two competing effects in locating the λ -transition: the lower effective temperature and larger effective thermal wavelength makes it more favorable, whereas the increased separation of closest approach between pairs of bosons makes it less favorable.

It should be mentioned that a hard-core potential was imposed with diameter inside the region in which the radial distribution function was anyway zero. It had no effect on the results. For example, the results at $k_B T/\varepsilon = 0.50$, $\rho\sigma^3 = 0.26$ with the hard-core diameter set at 1.40σ and at 1.28σ were statistically indistinguishable. The results in Table I were obtained with the hard-core diameter set at 1.18σ .

IV. CONCLUSION

The main point of this paper is to explore an approximation that reduces the complex phase space weight for a quantum system to a real weight in position config-

uration space. This is called the third order diagonal approximation, referring to the termination of the series for the Wigner-Kirkwood commutation function and to the projection of the quadratic momentum terms therein. The advantage is that the momentum integrals can be performed analytically rather than numerically as in the full third order approach.

For Lennard-Jones ^4He liquid below about 10 K, the subsequent Metropolis Monte Carlo simulation algorithm is found to be tractable. The algorithm and model seem to more readily solidify than real ^4He , and so results were obtained at a constant density that was about 25% less than the saturated liquid density at the lowest temperature studied, $T = 3.5\text{ K}$. The kinetic energy at $k_{\text{B}}T/\varepsilon = 0.5$ ($T = 5.1\text{ K}$) is about 25% lower than for the full third order numerical momentum quadrature approach. The energy, heat capacity, and radial distribution function have smaller error at this temperature and density.

That the present approach largely agrees with the earlier approach, and also the umbrella sampling result in Table I, tends to confirm the treatment of the complex phase space weight for a quantum system that was the basis of the original algorithm (Attard 2025h).

The present results were run for the same number of Monte Carlo steps as the earlier results, but took about 50% longer in computer time. Since the statistical error is about the same, we conclude that the present algorithm is slightly less efficient than the more exact numerical momentum quadrature algorithm.

Despite this, the analytic momentum quadrature of the third order diagonal approximation does offer a certain physical insight into the effects of the Wigner-Kirkwood commutation function, which embodies the Heisenberg uncertainty relation. It shows the link between momentum and position configuration that is missing in classical statistical mechanics. It shows quantitatively how the Heisenberg uncertainty relation increases the distance of closest approach of two bosons, and how the position configuration lowers the kinetic energy and the momentum state compared to the classical prediction.

One significant challenge with the classical phase space algorithm for the quantum Monte Carlo simulation of ^4He is that the model and level of approximation too readily produce solid phases at low temperatures. This precludes the exploration of the λ -transition in the saturated liquid. Of course the proximity to a solid phase is not unrealistic as real ^4He does become solid at low temperatures and elevated pressures, but it does frustrate the main goal of the simulations.

The problem appears to arise from the approximate nature of the short ranged, r^{-12} , repulsion in the Lennard-Jones pair potential, which is magnified with each successive gradient in the terms in the Wigner-Kirkwood commutation function. These shift the first peak in the radial

distribution function to larger separations and create an exclusion hole about each atom that greatly exceeds that given classically by the Lennard-Jones potential. In the case of the fourth order approximation to the Wigner-Kirkwood commutation function, even at half the measured saturation liquid density this causes solidification. The Lennard-Jones pair potential may well be optimized for the gas phase and for classical treatments, but in the quantum liquid regime a more reliable pair potential is called for. In this regard the pair potentials explored by Aziz *et al.* (1992) and used by Ceperley (1995), which were obtained from quantum calculations and gas phase measurements, may be more reliable.

References

- Attard P 2016b Quantum statistical mechanics as an exact classical expansion with results for Lennard-Jones helium arXiv:1609.08178v3
- Attard P 2018b Quantum statistical mechanics in classical phase space. Expressions for the multi-particle density, the average energy, and the virial pressure arXiv:1811.00730
- Attard P 2021 *Quantum Statistical Mechanics in Classical Phase Space* (Bristol: IOP Publishing)
- Attard P 2025a *Understanding Bose-Einstein Condensation, Superfluidity, and High Temperature Superconductivity* (London: CRC Press)
- Attard P 2025b The molecular nature of superfluidity: Viscosity of helium from quantum stochastic molecular dynamics simulations over real trajectories arXiv:2409.19036v5
- Attard P 2025h Quantum Monte Carlo in classical phase space with the Wigner-Kirkwood commutation function. Results for the saturation liquid density of ^4He arXiv:2512.09948
- Aziz R A, Slarnan M J, Koide A, Allnatt A R, and Meath W J 1992 Exchange-Coulomb potential energy curves for He-He, and related physical properties *Mol. Phys.* **77** 321
- Ceperley D M 1995 Path integrals in the theory of condensed helium *Rev. Mod. Phys.* **67** 279
- Donnelly R J and Barenghi C F 1998 The observed properties of liquid helium at the saturated vapor pressure *J. Phys. Chem. Ref. Data* **27** 1217
- Kirkwood J G 1933 Quantum statistics of almost classical particles *Phys. Rev.* **44**, 31
- van Sciver S W 2012 *Helium Cryogenics* (New York: Springer 2nd edition)
- Wigner E 1932 On the quantum correction for thermodynamic equilibrium *Phys. Rev.* **40**, 749